# Localized Three-Dimensional Functionalization of Bionanoreceptors on High-Density Micropillar Arrays via Electrowetting

Sangwook Chu,[†,‡] Thomas E. Winkler,[‡,§] Adam D. Brown,[§,∥] James N. Culver,[∥,⊥] and Reza Ghodssi*[†,‡,§]

[†]Department of Electrical and Computer Engineering, [‡]Institute for Systems Research, [§]Fischell Department of Bioengineering, [∥]Institute for Bioscience and Biotechnology Research, and [⊥]Department of Plant Science and Landscape Architecture, University of Maryland, College Park, Maryland 20742, United States

S *Supporting Information*

ABSTRACT: In this work, we introduce an electrowetting-assisted 3-D biofabrication process allowing both complete and localized functionalization of bionanoreceptors onto densely arranged 3-D microstructures. The integration of biomaterials with 3-D microdevice components offers exciting opportunities for communities developing miniature bioelectronics with enhanced performance and advanced modes of operation. However, most biological materials are stable only in properly conditioned aqueous solutions, thus the water-repellent proper-

ties exhibited by densely arranged micro/nanostructures (widely known as the Cassie−Baxter state) represent a significant challenge to biomaterial integration. Here, we first investigate such potential limitations using cysteine-modified tobacco mosaic virus (TMV1cys) as a model bionanoreceptor and a set of Au-coated Si-micropillar arrays (*μ*PAs) of varying densities. Furthermore, we introduce a novel biofabrication system adopting electrowetting principles for the controlled localization of TMV1cys bionanoreptors on densely arranged *μ*PAs. Contact angle analysis and SEM characterizations provide clear evidence to indicate structural hydrophobicity as a key limiting factor for 3-D biofunctionalization and for electrowetting as an effective method to overcome this limitation. The successful 3-D biofabrication is confirmed using SEM and fluorescence microscopy that show spatially controlled and uniform assemblies of TMV1cys on *μ*PAs. The increased density of TMV1cys per device footprint produces a 7-fold increase in fluorescence intensity attributed to the *μ*PAs when compared to similar assemblies on planar substrates. Combined, this work demonstrates the potential of electrowetting as a unique enabling solution for the controlled and efficient biofabrication of 3-D-patterned micro/nanodomains.
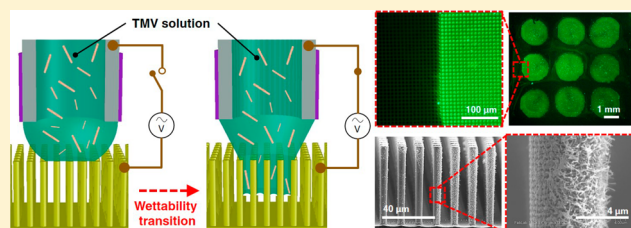
■ INTRODUCTION

The convergence of biochemistry and micro/nanomanufacturing technologies has resulted in revolutionary advancements in the development of miniaturized devices and systems equipped with novel functions derived from biomaterials such as nucleic acids, antibodies, enzymes, and viruses.[1,2] The integration of these biomaterials into devices has positively impacted numerous applications that include sensors, gene discovery platforms, and bioenergy production.[1,3] However, despite these advancements there remains a need for new strategies that permit the controlled deposition and patterning of functional biomaterials onto device surfaces.

Some of the representative approaches and technologies developed previously for biopatterning include (1) the use of conventional lithography techniques (e.g., UV, E-beam, and FIB) to create heterogeneous surface patterns for the selective functionalization of biomaterials,[4−6] (2) microcontact printing (*μ*CP) which adopts the scheme of traditional ink stamps with PDMS-based microgratings for biopattern transfer at submicrometer resolution,[7,8] and (3) dip-pen nanolithography (DPN) which utilizes atomic force microscopy systems to draw nanoscale biopatterns, leveraging their ultrahigh mechan-

ical precision.[9] Such biofabrication technologies have rapidly evolved over the past two decades based on biochemical principles, micro/nanofabrication processing methodologies, and instrumentation science/engineering. The development of these biofabrication technologies has led to a greater understanding of biomolecular activities through on-chip characterization and enables the rapid development of advanced bioelectronics including biosensors and bioenergy harvesters.[1,10]

Recent efforts have demonstrated the integration of biomaterials with 3-D transducers for enhanced performance or advanced modes of operation for bioelectronics on miniaturized scales.[11−15] Three-dimensional structures at micro- and nanoscales offer numerous beneficial properties compared to their 2-D counterparts. The primary attractive feature is their expanded physical interface between system components and materials which can directly translate into a significant enhancement in respective performance. Also,

precise pattern control over these interfaces using micro/nanofabrication or emerging 3-D printing technologies has the potential to further improve the surface-to-volume ratio, functional uniformity, and tunability of these devices.[16]

One of the interesting characteristics present in such small-scale 3-D structures is their limited wetting, known as structural hydrophobicity or the Cassie−Baxter wetting state.[17−20] When micro-/nanoscale structures are densely arranged, the wetting of 3-D microcavities with aqueous liquids can be hindered by the balancing of surface tensions at the solid−liquid, solid−gas, and liquid−gas interfaces.[21] Considering that most biological materials are stored in buffered aqueous solutions due to inherent narrow biological stability windows, such limited wetting properties can become a significant obstacle when attempting to build and pattern 3-D interfaces between devices and biomaterials.[22,23] Over the past decade, our group has been developing miniaturized device components (microenergy storage devices and bio/chemical sensors) utilizing genetically modified tobacco mosaic virus (TMV1cys) as a nanoscale functional material.[24,25] In recent efforts, we have demonstrated the use of TMV1cys-based hierarchical electrodes for electrochemical charge storage devices achieving a significant increase in performance.[22,25] However, we have encountered challenges when functionalizing TMV1cys on high-density microstructures, which limited our ability to further increase the area-to-volume ratio of our devices with enhanced performance.

Among the effective methods to induce structural wettability (the Cassie−Baxter to Wenzel state) is the widely applied principle of electrowetting.[19,26] Electrowetting allows one to control material wetting states by the modulation of applied electric potential at the solid−liquid interface. Due to its high precision over the manipulation of liquid droplets on solid surfaces, it has been utilized for a wide range of applications including liquid-based optical components,[27] new display technologies,[28] and digital microfluidics.[29] More importantly for this work, electrowetting for wettability transition in various 3-D structured materials (e.g., Si nanoposts,[30] epoxy microposts,[31] and carbon nanotubes (CNT)[32]) has been demonstrated. However, to the best of our knowledge, this principle has not yet been applied for the wetting of biological solutions into 3-D structured materials for surface functionalization.

In this report, we characterize and identify structural hydrophobicity as a key limiting factor in the successful 3-D biofunctionalization of patterned microsurfaces and introduce an electrowetting-assisted biofabrication technology that allows for the complete and localized assembly of TMV1cys onto structurally hydrophobic substrates. Specifically, Si-based micropillar array (μPA) electrodes having different pillar spacings were used to investigate the relationship between μPA densities to the extent of TMV1cys functionalization on these 3-D surfaces. The electrowetting principle is revealed as an enabling solution for 3-D biofabrication, displaying enhanced abilities to integrate functionalized biological macromolecules onto micropatterned surfaces. Overall, the biofabrication process introduced and characterized in this work provides a basic resource and suggests potential opportunities for the development of advanced biointegrated 3-D devices and systems.

■ EXPERIMENTAL SECTION

Cysteine-Modified TMV1cys and Self-Assembly onto Au Surfaces. TMV is a cylindrical plant virus featuring high-aspect-ratio geometry with a 300 nm length, 18 nm outer diameter, and 4 nm inner channel diameter. The structure is a result of ∼2130 coat proteins encapsulating an RNA genome. Driven by genetic modification and chemical conjugation strategies, TMV has been engineered over the past decade to provide nanoscale biological templates for assembling a wide range of nanostructured materials (metals,[33,34] metal oxides,[22,25] polymers,[35] peptides,[36] enzymes,[37] etc.) for developing energy storage devices, bio/chemical sensors, drug-delivery molecules, etc. The biomaterial used in this work is genetically modified TMV expressing thousanda s of cysteine residues on its outer surface (for TMV1cys, the details of genetic modification and purification protocols can be found in a previous report[33]). A 0.2 mg/ml concentration of TMV1cys in 0.1 M, pH 7 phosphate buffer (PB) solution is used for all experiments. The increased metal binding properties of TMV1cys, such as self-assembly onto Au surfaces and surface metallization with Ni,[23] and its facile chemical binding sites for fluorescent conjugation provide a great means for the characterization of functionalization morphology and biochemical activity after the electrowetting-assisted biofabrication process.

Au-Coated Si μPA as Structurally Hydrophobic Substrates. As shown in Figure 1a, a set of four different μPA electrodes is
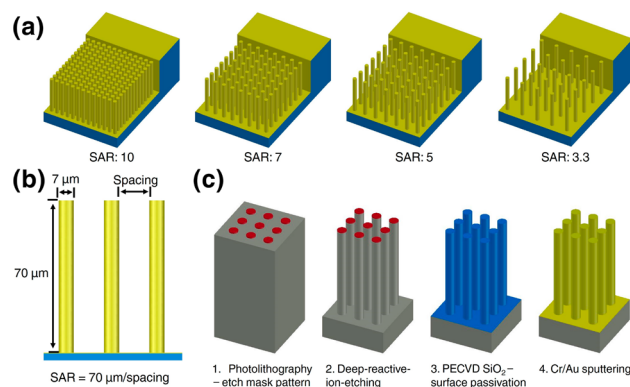

Figure 1. (a) Schematics of Au-coated Si-μPA electrodes featuring a range of SARs. (b) Cross-sectional view of the μPA with geometrical parameters; the pillar aspect ratio remains at 10 for all electrodes while the spacing varies from 7 to 21 μm for SARs of 10, 7, 5, and 3.3. (c) Fabrication process involving one-step photolithography followed by DRIE. The Cr/Au electrodes are deposited via sputtering with an underlying SiO₂ passivation layer deposited via PECVD.

fabricated to study the dependence of TMV1cys functionalization on the μPA density using a previously reported method that involves the complete immersion of respective electrodes into TMV1cys solution followed by 18 h of incubation for the self-assembly. All pillars are 70 μm tall and 7 μm in diameter, but the spacing between the pillars is varied from 7 to 21 μm, allowing the spacing aspect ratio (SAR) to vary from 10 to 3.3 (Figure 1b). Figure 1c illustrates the fabrication process for the μPA electrodes. A silicon substrate is patterned with a negative photoresist (NR9-1500PY, Futurrex) etch mask and etched using deep reactive ion etching (DRIE; STS deep reactive ion etcher). The etched wafer is diced into single chips (1 × 1.7 cm^2 with a 1 × 1 cm^2 pillar array area), and the surface is passivated with SiO₂ (500 nm at 300 °C) using plasma-enhanced chemical vapor deposition (PECVD, Oxford Plasmalab System 100). Electrodes are created by subsequent sputter deposition (model AJA International, ATC 1800-V) of Ti (30 nm)/Au (120 nm).

Electroless Ni Metallization for SEM Characterization. The SEM (Hitachi S-3400) characterization of surface-immobilized TMV1cys leverages electroless Ni metallization of the viral macromolecules prior to imaging. The process involves an initial 5 h surface activation step in Pd solution (0.7 mM Na₂PdCl₄ in 0.1 M PB solution), creating Ni nucleation sites, followed by a 4 min immersion in Ni solution (50 mM NiCl₂, 75 mM Na₂B₄O₇, 0.13 M glycine, and 0.25 M (CH₃)₂NHBH₃ in deionized water). The process is carried out

under ambient conditions. The details of the solution preparation protocols can be found in previous reports.[23,33]

Fluorescence Microscopy Characterization. The increased biochemical density of 3-D-functionalized TMV1cys on μPA electrodes was evaluated by labeling thiols (on exposed cysteine residues) with a 50 μg/mL fluorescent labeling reagent (fluorescent 5-maleimide) prepared in 0.1 M PB solution (pH 7). The TMV1cys-functionalized electrodes were immersed in the labeling solution for 2 h and then repeatedly rinsed with deionized water before imaging (Leica INM100). The acquired fluorescence images were evaluated using open source image analysis software ImageJ.

System Components for Electrowetting-Assisted Three-Dimensional Biofabrication. A custom-built setup was developed to characterize and implement the electrowetting of TMV1cys solutions onto high-density (SAR = 10) μPA electrodes. Figure 2a
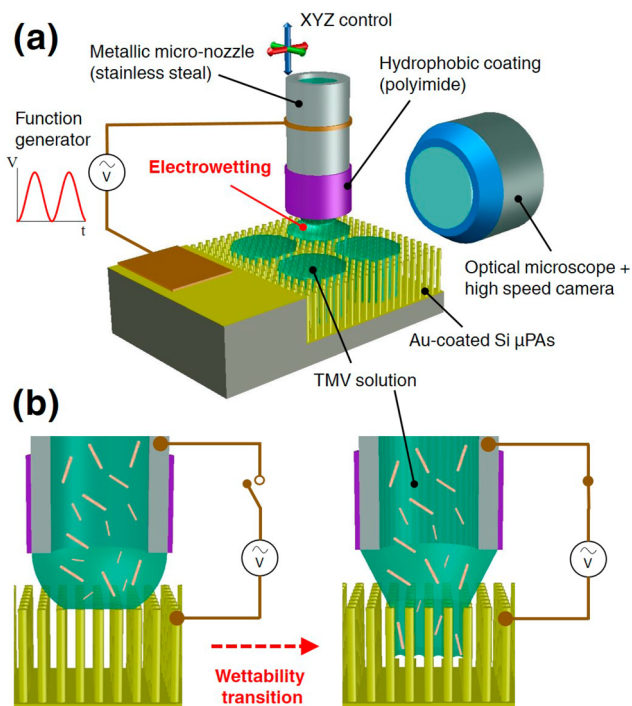

Figure 2. (a) Overview of the custom-built system for the electrowetting-assisted 3-D biofabrication process and (b) cross-sectional schematics describing the electrowetting-induced structural wettability transition and the introduction of TMV1cys into the deep microcavities.

illustrates an overview of the developed system comprising six major elements: (1) TMV1cys solution, (2) a Au-coated Si μPA electrode, (3) a stainless-steel nozzle with its tip coated with a hydrophobic film (polyimide), (4) an ac function generator (Agilent 33220A), (5) an XYZ micromanipulator (Velmex modules), and (6) an optical microscope with high-speed image capture capability (Redlake MotionPro HS-3). The electrowetting process is conducted in air at room temperature. The details of each element are described below.

The TMV1cys solution functions as a biological ink to be functionalized and patterned on the μPAs. As mentioned before, the TMV1cys used in this work is genetically modified with cysteines, which contain thiol groups (-SH), on their surfaces. This allows TMV1cys macromolecules to self-assemble onto Au surfaces through Au-thiol binding as well as uniform metallization over their nanoscale structure through electroless plating.[33] This is critical to the successful demonstration of this approach, allowing the characterization of functionalization morphology and biochemical activity after the electrowetting process via SEM and fluorescent labeling.

The μPA electrode serves as a 3-D substrate in the system. The hydrophobicity provides physical control over the wetting and

patterning process by limiting the substrate wetting at thermal equilibrium. The Au layer used to coat the Si pillar structure functions as an electrode for the electrowetting process as well as a means for the functionalization of the cysteine-modified TMV1cys through the Au-thiol binding mechanism. Considering the hydrophobicity of the substrate, it is challenging to accurately position the TMV1cys solution on the μPAs and even more problematic when the volume of the solution is in the microliter range. This is overcome by the use of a modified metallic nozzle and the XYZ micromanipulator positioned over the substrate. Specifically, the hydrophobic film (polyimide) coating the outer surface of the metallic nozzle enables the formation of a semispherical hanging drop of the biological solution. This key modification allows precise control over the amount of solution dispensed during each electrowetting step (∼1 μL/electrowetting). Without the coating, the dispensed liquid would immediately roll upward to the outer metallic surface, hence making it challenging to control the size and amount of solution used for the electrowetting step.

The cross-section of the electrowetting step is described in Figure 2b. As shown in the left panel, the TMV1cys solution at the nozzle adopts the Cassie−Baxter state when it is loaded onto the μPAs (Figure 2b, left). When the electrowetting voltage is applied, an instant transition in surface wettability is induced, driving the TMV1cys solution into the microcavities (Figure 2b, right), transitioning to the Wenzel state.[19] This allows uniform self-assembly/functionalization of TMV1cys onto the surfaces of the deep microstructures.

In order to apply the electrowetting voltage at the solid−liquid interface formed at the tip of the pillars, an ac function generator is directly connected to the μPAs and the stainless-steel part of the nozzle. Using the horizontally positioned microscope, the dynamics of the electrowetting are characterized by monitoring the apparent contact angle for a range of applied voltage levels. The frequency of the applied voltage was kept at 10 kHz to avoid bubble generation from the electrolysis of water.

■ RESULTS AND DISCUSSION

TMV1cys Assembly on μPAs of Different Densities. As an initial step, the structurally hydrophobic properties of Au-coated μPAs are characterized via contact angle measurements of 10 μL sessile drops of the TMV1cys solution on Au-coated planar (Figure 3a) and μPA electrodes (Figure 3b). While the
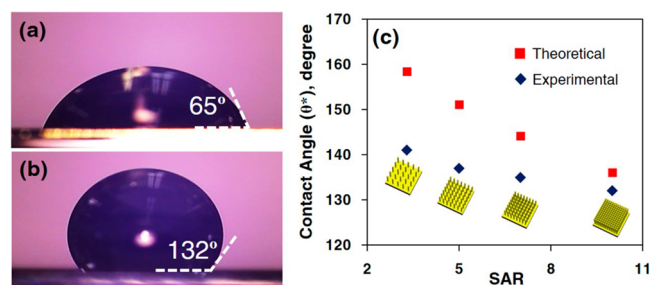

Figure 3. Comparison of apparent contact angle measurements of 10 μL sessile drops of TMV1cys solution (0.2 mg/mL in 0.1 M PB solution) on Au-coated (a) planar and (b) μPA (SAR = 10) electrodes. (c) The experimentally measured contact angles (θ^*) follow a theoretically expected trend while there is increasing disparity with lower SARs.

planar Au surface exhibits a hydrophilic nature with a 65° contact angle, the μPAs yield higher hydrophobic characteristics as indicated by a 132° contact angle (the Cassie−Baxter state). This is close to the theoretically expected value (136°) calculated on the basis of the Cassie−Baxter equation (eq 1), where θ^* is the apparent contact angle on the μPAs, ϕ_s is the

fraction of the solid in contact with the TMV1cys solution, and θ_0 is the contact angle on the planar Au substrate.[19]

$$\cos \theta* = -1 + \phi_s(1 + \cos \theta_0) \qquad (1)$$

Figure 3c plots both theoretically expected (derived from Cassie−Baxter eq 1 with $\theta_0 = 65°$ and ϕ_s calculated from the pillar geometry) and experimentally acquired contact angles ($\theta*$) indicating that the hydrophobicity of the μPAs decreases with an increase in SAR. The disparity between the two can be attributed to the gentle pressure applied when loading the droplet onto the μPAs via syringe tips and a hydrophilic surface (Au), inducing liquid pinning onto the pillar tips.[38] Such a wetting state is valid only when there is no external disruption force due to the hydrophilicity of the Au surface. Once the Cassie−Baxter state is disrupted with an external force (e.g., mass loading), a faster transition of the wetting state, indicated by the droplet spreading into the cavities (transitioning to the Wenzel state), is observed with the lower SAR μPAs (data not shown). It becomes significantly challenging to introduce the solution into narrower cavities (SAR ≥ 7) that do not easily transition to a Wenzel state, attributed to less pressure loading per each spacing segment. In other words, the wider spacing reduces ϕ_s, which as a result increases the fraction of the liquid droplet that is supported by the micropillars.[18,38] The TMV1cys droplets on such high SAR μPAs are readily movable with no traceable liquids remaining on the electrode surface.

The wetting properties discussed above are experimentally represented in the following SEM characterizations. The Au-coated Si μPAs having different densities (Figure 1a) are functionalized with TMV1cys using the previously reported method where each electrode is immersed in 1 mL of TMV1cys solution and incubated for 18 h at room temperature for self-assembly through thiol−Au binding. The surface functionalization morphologies are characterized using cross-sectional SEM (Figure 4) after electroless metallization with Ni. Figure 4a−d compares the TMV1cys textured pillar sidewalls that are
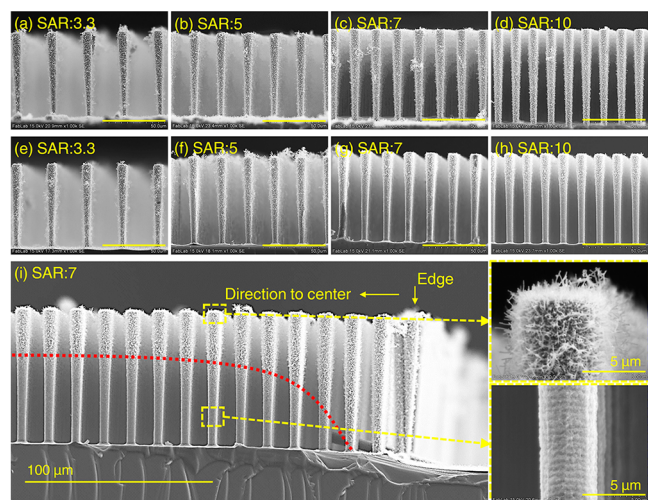
located on the edge of the electrodes. As clearly observed, a complete and uniform coverage of the vertical sidewalls with TMV1cys-based nanostructures is observed irrespective of the density. However, when examining the pillars located in the central region of the μPAs (Figure 4e−h), a gradual reduction of TMV1cys surface coverage toward the bottom of the pillars is observed with increased SAR. Uniform TMV1cys assembly was achieved only on pillar arrays with a SAR of 3.3 (Figure 4e). In addition, for the μPAs having a SAR above 5, the TMV1cys functionalization created a profile from the edge toward the array center (red-dotted curve in Figure 4i; representative image from SAR = 7), indicating that the wetting of the liquid is strongly limited in the high SAR cavities as it experiences a greater sum of surface tensions while spreading through the closely spaced micropillar sidewalls− resulting in a reduced capillary pressure in the radial spreading direction. The combined results strongly imply that the Cassie−Baxter wetting property of densely arranged μPAs can limit biomaterial integration into densely packed micropillar arrays.

Electrowetting Dynamics of TMV1cys Solutions on μPAs. For these experiments, electrowetting for 3-D biofunctionalization was performed using the custom-built system introduced in the Experimental Section. μPAs featuring a SAR of 10 were used to control structural hydrophobicity for electrowetting and to achieve high-density TMV1cys immobilization per device footprint. First, the electrowetting voltage is characterized by monitoring the change in droplet configuration (TMV1cys solution) upon wetting and measuring the steady-state contact angle at different applied voltages. Figure 5 compares the steady-state contact angles of TMV1cys droplets on planar Au (Figure 5a) and Au-coated μPA substrates (Figure 5b). The applied ac voltages are varied from 0 to 1.2 V_{RMS}, featuring a 0 minimum level with the peak-to-peak amplitude varying from 0 to 2 V_{PP} at 10 kHz, and the steady-state contact angles are measured 3 s after the surface impingement. (No noticeable spreading is observed at this time point.) As expected, the droplet on a planar Au substrate shows hydrophilic contact angles for all applied voltage levels with slightly lower measures at increased voltages. However, a droplet impinging the μPA substrate shows a slower and more gradual decrease in contact angle as the voltage is increased, demonstrating the higher dependency of its wettability on the electrowetting voltage compared to the planar counterpart. (See Video S1−S3.)

Figure 6a,b shows the change in contact angle monitored over time until it reached steady state, to characterize the electrowetting dynamics. As shown, there is an abrupt change in the contact angle of the liquid drops impinging a planar surface, reaching the steady-state contact angle within a second (Figure 6a). The steady-state angles line up with very small differences corresponding to the level of applied voltages. (180° is plotted to indicate the abrupt change—it is the tangent angle for the hemispherical droplet right before impingement.) Figure 6b plots the change in contact angle on the μPAs. The primary observation is that the higher voltage induced a faster change in contact angle due to the increased applied capacitive energy at the solid−liquid interface. In addition, the electrowetting on μPAs shows three distict dynamic regions over time. First, an abrupt change in contact angle is induced upon the application of the electrowetting voltage due to an instant reduction of the surface tension at the solid−liquid interface. However, this is not as abrupt as observed on the
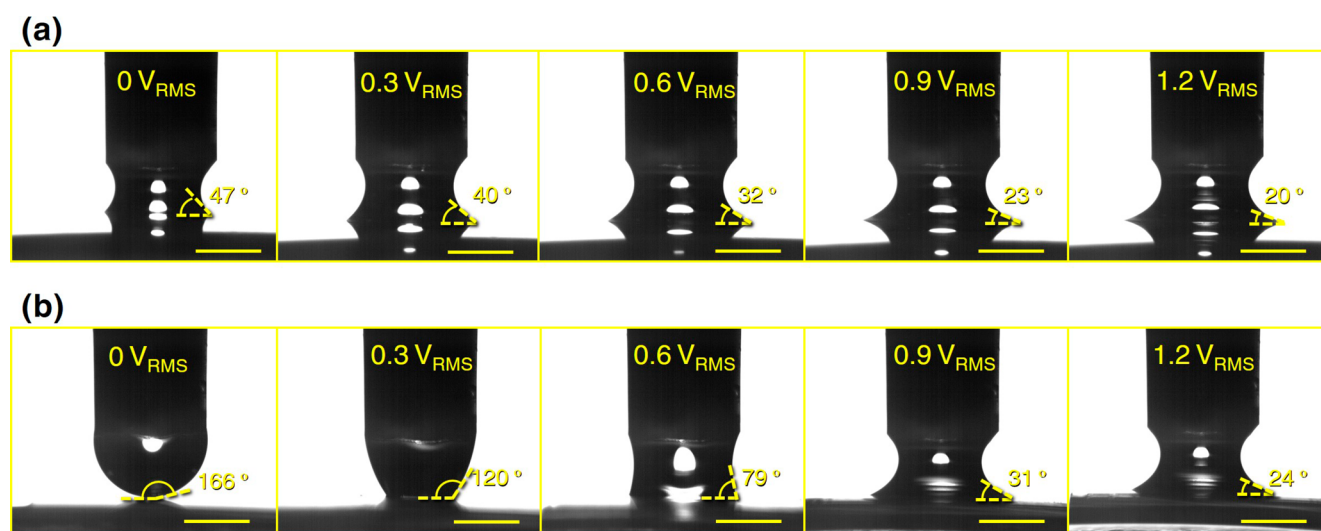

Figure 4. Cross-sectional SEM images of the μPAs functionalized with TMV1cys using the previously reported method[23] (scale bars: 50 μm unless specified). (a−d) SEM images taken at the very edge of the four electrodes and (e−h) taken at the electrode center area after cleaving. (i) A functionalization profile (red-dotted curve) is created from the edge to the center of the electrodes having SAR > 5 due to the limited structural wetting.

Figure 5. Comparisons of steady-state contact angles on Au-coated (a) planar and (b) μPA (SAR = 10) electrodes (scale bars: 1 mm). Images were taken 3 s after applying the specified electrowetting voltages.
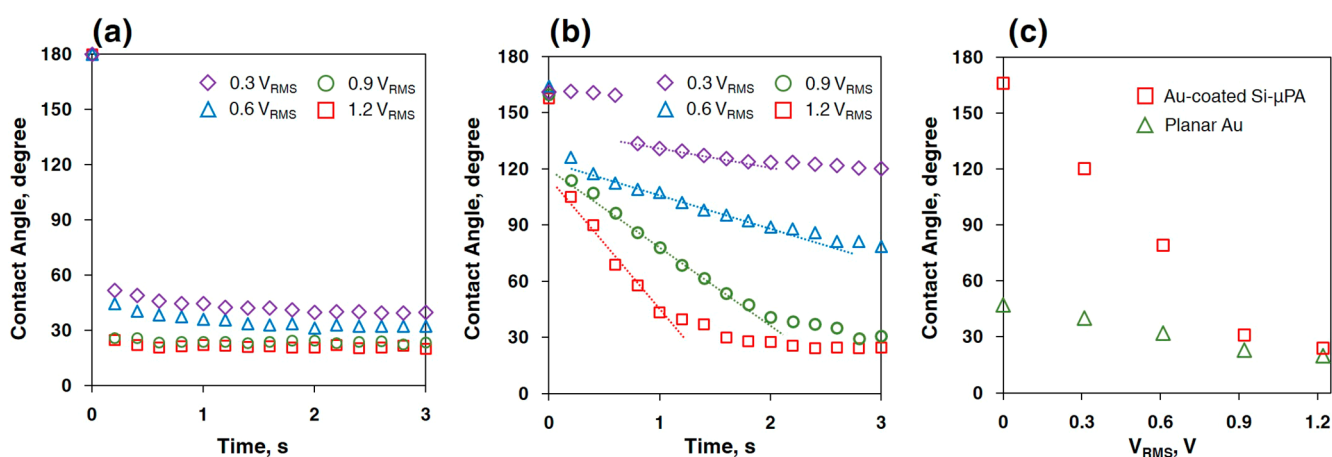

Figure 6. Comparisons of the change in contact angle over time at different electrowetting voltages on Au-coated (a) planar and (b) μPA (SAR = 10) electrodes. (c) Comparison of steady-state contact angles measured from planar and μPA electrodes indicate 1.2 V_{RMS} as a complete wetting voltage.

planar surface as the radial spreading is more hindered by the surface tentions formed at the pillar side wall−liquid interfaces. As a result, a semilinear region (indicated by the straight dotted lines on the graphs) is followed where the wetting boundary spreads gradually in the radial direction as the liquid reaches the bottom surface. This in the end transitions into a saturated region as the contact angle approaches a steady state, in which the wetting does not involve a change in contact angle. (The spreading of liquid in the radial direction continues within the microcavities based on visual observation, assigned to capillary pressure.[26]) Overall, this characterization confirms that the wetting of liquid within 3-D structures can be controlled by adjusting the voltage amplitude and duration of electrowetting, thereby indicating the capability to control the biofunctionalization of 3-D substrates.

The electrowetting voltage of 1.2 V_{RMS} at 10 kHz was identified as optimal for TMV1cys solution wetting, as determined from the steady-state contact angle measured from the planar Au and the μPA substrates as shown in Figure 6c. Basically, the voltage level that reached a similar contact angle between the two substrates was chosen, as this is

considered to be indicative of complete wetting. Lower electrowetting voltage levels (<1.2 V_{RMS}) would leave exposed pillar surfaces at the bottom of the microcavities. Also, the ac voltage signal significantly helped minimize electrolysis/bubble generation during electrowetting; when observed with the microscope, there was no observable bubble generation with the ac voltage, while a dc voltage of 1.2 V created noticeable bubbles on electrode surfaces and within the TMV1cys droplet during the electrowetting process, which can hinder successful biofunctionalization.

Localized Three-Dimensional Functionalization of TMV1cys on μPAs. The morphology of electrowetting-processed TMV1cys on μPAs was characterized using SEM after electroless Ni metalization. The cross-sectional images taken from these μPAs confirm complete and uniform TMV1cys nanotexturing of the μPAs (Figure 7a). Compared to our previous methods using complete immersion of the substrates in 1 mL of a TMV1cys solution bath (Figure 4h), this is a significant improvement considering the excellent uniformity of the TMV1cys coating at the lower and deep portion of the μPA surfaces. Figure 7b shows the μPAs that are
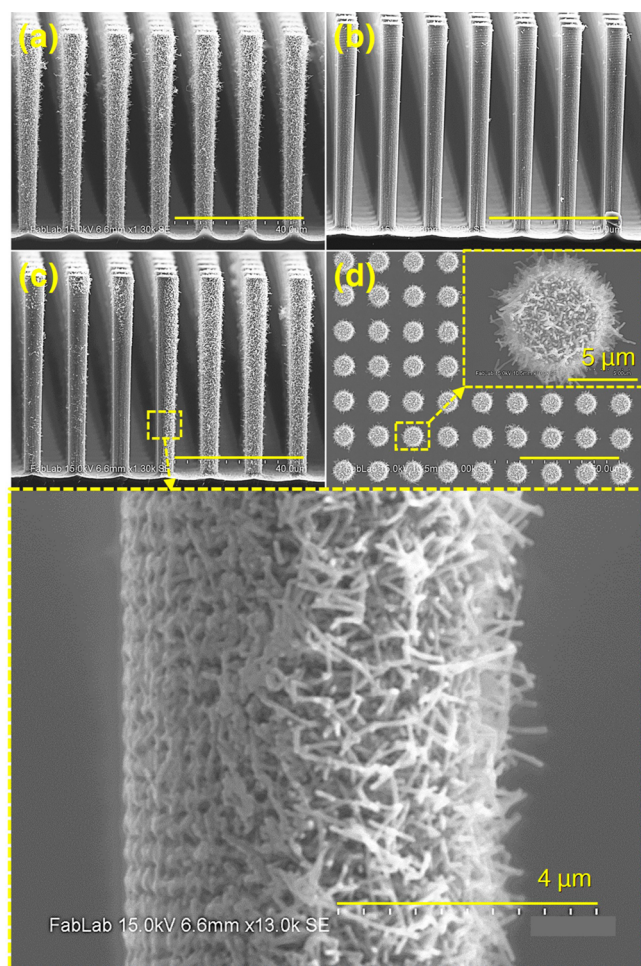
Figure 7. SEM images of μPA electrodes (SAR = 10) with Ni-coated TMV1cys nanostructures (scale bars: 40 μm unless specified). (a) The electrowetting allowed a complete TMV1cys coverage along the deep micropillar side walls compared to the (b) nonelectrowetted μPAs. (c) A clear functionalization boundary formed along a single pillar surface at the wetting edge. (d) Top-down view of the μPAs showing a uniform TMV1cys coverage across the electrowetting-processed μPAs.

exposed to a TMV1cys droplet without electrowetting. Only isolated TMV1cys macromolecules coated with Ni are observed at the top surfaces of the pillars while most of the micropillar surfaces remain uncovered. This indicates that the Cassie–Baxter state of the droplet is stable through the overnight self-assembly process and increases the significance of the electrowetting-assisted process as an enabling technology.

Figure 7c shows the μPAs located at the wetting edge. Corresponding to the optical microscope image provided in Figure S1, a clear functionalization boundary is formed on a side wall of micropillars located along the wetting edge. The initial limitation from the structural hydrophobicity plays a critical role in locally confining TMV1cys functionalization on the 3-D substrate by limiting the lateral spreading of liquid with reduced radial capillary pressure, which is a result of the increased sum of solid–liquid surface tensions owing to the densely arranged vertical pillar side walls. Additional top-down SEM images (Figure 7d) showing the tops of TMV1cys-assembled micropillars further demonstrate the beneficial utility of electrowetting principles for creating uniform biofunction-alized hierarchical device components.

As a final characterization, the biochemical activity of TMV1cys assembled by electrowetting was evaluated using a sulfhydryl (−SH)-specific fluorescent labeling reagent, fluo-rescein-5-maleimide. Figure 8a,b compares the fluorescence emitted by labeled TMV1cys macromolecules on planar Au and μPA substrates, respectively. Fluorescent microscope settings were identical for both images (e.g., magnification, exposure time, etc.). As clearly observed, a significant increase in the fluorescence intensity is achieved with the hierarchically arranged TMV1cys on the μPAs, attributed to the increased nanoreceptor density within the functionalization area. The image analysis indicated an ~7-fold increase in the intensity (Figure 8c), a significant enhancement enabled by successful TMV1cys integration with the high-density microstructures. The enhancement factor achieved is slightly less than the theoretically expected value of 8.9 (derived on the basis of the μPA geometry[25]). Potential reasons are (1) a wider focal depth for the 3D structure compared to the planar substrate and (2) possible emission losses within the volume of the μPAs.
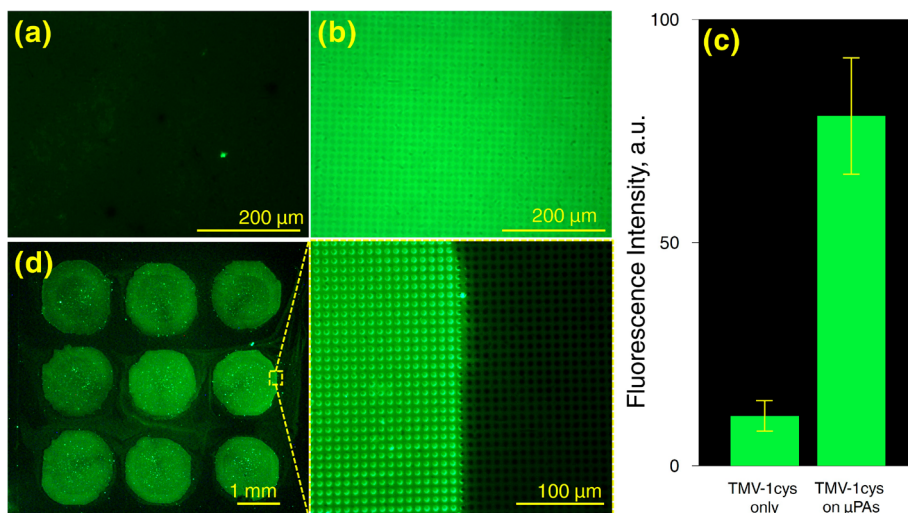

Figure 8. Fluorescence microscopy characterization confirming the biochemical activity of TMV1cys after electrowetting. Comparing TMV1cys on (a) planar and (b) μPAs, (c) a 7-fold increase in fluorescence intensity is achieved (n = 9), with excellent functionalization uniformity and pattern fidelity across the (d) 3 × 3 arrays of hierarchical bionanoreceptors.

Furthermore, in efforts to demonstrate the patterning capability of the developed biofabrication system (Figure 2a), 3 × 3 hierarchical TMV1cys arrays on 7 × 7 mm² μPA substrates were fabricated as shown in Figure 8d. As indicated by the error bars in Figure 8c, the TMV1cys arrays fabricated through the electrowetting process show excellent uniformity in biochemical activity. The results combined demonstrate the advantages of the electrowetting-assisted 3-D biofabrication technology for building multiplexed and high-throughput bio/chemical sensing/analysis platforms.

While the introduced biofabrication platform and the demonstrated results sufficiently validate the applicability of electrowetting for biomaterial patterning on 3-D electrodes, there are a range of additional opportunities to further develop this approach in terms of scalability, programmability, composition of biomaterials, and complexity of 3-D substrates. For instance, the use of smaller-capillary nozzles and/or nanoscale 3-D substrates can allow enhanced pattern resolution and increased array density. Also, further integration with automated mechanical systems with multiple nozzles can enable programmable and high-throughput 3-D biofabrication technology for the production of arrayed or multiplexed biointegrated devices and systems.

SUMMARY AND CONCLUSIONS

This work reports the characterization of the TMV1cys assembly on Au-coated Si-μPAs having different densities and identifies structural hydrophobicity as a key limiting factor for 3-D biofunctionalization. A major breakthrough of this study was achieved by adopting electrowetting principles, which circumvented structural hydrophobicity limitations to enable the controlled patterning of 3-D assembled bionanoreceptors on high-surface-area microstructures. Results from this study demonstrate the potential of electrowetting technologies to serve as robust platforms for the biofabrication of micro/nano/biointegrated 3-D devices and systems. These findings offer new possibilities for developing advanced 3-D components beneficial for a range of microdevice applications including microenergy storage/harvesting, biochemical sensing, microthermal management, water-repellent surfaces, etc. The simple principles, readily available system components, and minimal volumes of biological solutions featured by the custom-built fabrication system suit the major criteria for widespread application of this technology.

ASSOCIATED CONTENT

ⓢ Supporting Information

The Supporting Information is available free of charge on the ACS Publications website at DOI: 10.1021/acs.langmuir.7b02920.

> Figure S1. Cross-sectional optical microscopy of wetting edge (TMV1cys solution on Au-coated Si μPAs (SAR = 10)). (PDF)
> Video S1. Electrowetting on a planar Au substrate. (AVI)
> Video S2. Electrowetting on Au-coated Si μPAs (SAR = 10). (AVI)
> Video S3. TMV1cys droplet impinging on Au-coated Si μPAs (SAR = 10) without electrowetting. (AVI)

AUTHOR INFORMATION

Corresponding Author

*E-mail: ghodssi@umd.edu. Phone: +1 301-405-8158.

ORCID

Sangwook Chu: 0000-0002-1173-6377

Notes

The authors declare no competing financial interest.

REFERENCES

(1) Liu, Y.; Kim, E.; Ghodssi, R.; Rubloff, G. W.; Culver, J. N.; Bentley, W. E.; Payne, G. F. Biofabrication to Build the Biology-Device Interface. *Biofabrication* **2010**, *2* (2), 022002.

(2) Calò, A.; Eiben, S.; Okuda, M.; Bittner, A. M. Nanoscale Device Architectures Derived from Biological Assemblies: The Case of Tobacco Mosaic Virus and (Apo)ferritin. *Jpn. J. Appl. Phys.* **2016**, *55* (3S2), 03DA01.

(3) Schena, M.; Heller, R. A.; Theriault, T. P.; Konrad, K.; Lachenmeier, E.; Davis, R. W. Microarrays: Biotechnology's Discovery Platform for Functional Genomics. *Trends Biotechnol.* **1998**, *16* (7), 301−306.

(4) Makohliso, S. A.; Giovangrandi, L.; Léonard, D.; Mathieu, H. J.; Ilegems, M.; Aebischer, P. Application of Teflon-AF® Thin Films for Bio-Patterning of Neural Cell Adhesion. *Biosens. Bioelectron.* **1998**, *13* (11), 1227−1235.

(5) Bergman, A. A.; Buijs, J.; Herbig, J.; Mathes, D. T.; Demarest, J. J.; Wilson, C. D.; Reimann, C. T.; Baragiola, R. A.; Hu, R.; Oscarsson, S. O. Nanometer-Scale Arrangement of Human Serum Albumin by Adsorption on Defect Arrays Created with a Finely Focused Ion Beam. *Langmuir* **1998**, *14* (24), 6785−6788.

(6) Kumagai, S.; Yoshii, S.; Yamada, K.; Fujiwara, I.; Matsukawa, N.; Yamashita, I. Nanopatterning of Vapor-Deposited Aminosilane Film Using EB Lithography for Ferritin Protein Adsorption. *J. Photopolym. Sci. Technol.* **2005**, *18* (4), 495−500.

(7) Pla-Roca, M.; Fernandez, J. G.; Mills, C. A.; Martínez, E.; Samitier, J. Micro/nanopatterning of Proteins via Contact Printing Using High Aspect Ratio PMMA Stamps and Nanoimprint Apparatus. *Langmuir* **2007**, *23* (16), 8614−8618.

(8) Filipponi, L.; Livingston, P.; Kašpar, O.; Tokárová, V.; Nicolau, D. V. Protein Patterning by Microcontact Printing Using Pyramidal PDMS Stamps. *Biomed. Microdevices* **2016**, *18* (1),10.1007/s10544-016-0036-4.

(9) Lee, K.-B.; Park, S.-J.; Mirkin, C. A.; Smith, J. C.; Mrksich, M. Protein Nanoarrays Generated By Dip-Pen Nanolithography. *Science (Washington, DC, U. S.)* **2002**, *295* (5560), 1702.

(10) Rasmussen, M.; Abdellaoui, S.; Minteer, S. D. Enzymatic Biofuel Cells: 30 Years of Critical Advancements. *Biosens. Bioelectron.* **2016**, *76*, 91−102.

(11) Shi, L.; Chu, Z.; Liu, Y.; Peng, J.; Jin, W. Three-Dimensional Porous Microarray of Gold Modified Electrode for Ultrasensitive and Simultaneous Assay of Various Cancer Biomarkers. *J. Mater. Chem. B* **2014**, *2* (18), 2658−2665.

(12) Branch, B.; Schei, J. L.; Gupta, G.; Dattelbaum, A. M.; Petsev, D. N.; George, J. S. Micropillar Electrode Array: From Metal to Dielectric Interface. *IEEE Sens. J.* **2015**, *15* (9), 4992−5000.

(13) Liu, J.; Wang, J.; Wang, T.; Li, D.; Xi, F.; Wang, J.; Wang, E. Three-Dimensional Electrochemical Immunosensor for Sensitive Detection of Carcinoembryonic Antigen Based on Monolithic and Macroporous Graphene Foam. *Biosens. Bioelectron.* **2015**, *65*, 281−286.

(14) Penmatsa, V.; Ruslinda, A. R.; Beidaghi, M.; Kawarada, H.; Wang, C. Platelet-Derived Growth Factor Oncoprotein Detection Using Three-Dimensional Carbon Microarrays. *Biosens. Bioelectron.* **2013**, *39* (1), 118−123.

(15) Inan, H.; Poyraz, M.; Inci, F.; Lifson, M. A.; Baday, M.; Cunningham, B. T.; Demirci, U. Photonic Crystals: Emerging

Biosensors and Their Promise for Point-of-Care Applications. *Chem. Soc. Rev.* **2017**, *46*, 366.

(16) Vaezi, M.; Seitz, H.; Yang, S. A Review on 3D Micro-Additive Manufacturing Technologies. *Int. J. Adv. Manuf. Technol.* **2013**, *67* (5−8), 1721−1754.

(17) Zhang, X.; Shi, F.; Niu, J.; Jiang, Y.; Wang, Z. Superhydrophobic Surfaces: From Structural Control to Functional Application. *J. Mater. Chem.* **2008**, *18* (6), 621−633.

(18) Tuteja, A.; Choi, W.; Ma, M.; Mabry, J. M.; Mazzella, S. a; Rutledge, G. C.; McKinley, G. H.; Cohen, R. E. Designing Superoleophobic Surfaces. *Science* **2007**, *318* (5856), 1618−1622.

(19) Bahadur, V.; Garimella, S. V. Electrowetting-Based Control of Static Droplet States on Rough Surfaces. *Langmuir* **2007**, *23* (9), 4918−4924.

(20) Zhao, Y.-P.; Yuan, Q. Statics and Dynamics of Electrowetting on Pillar-Arrayed Surfaces at the Nanoscale. *Nanoscale* **2015**, *7* (6), 2561−2567.

(21) Lafuma, A.; Quéré, D. Superhydrophobic States. *Nat. Mater.* **2003**, *2* (7), 457−460.

(22) Chu, S.; Gerasopoulos, K.; Ghodssi, R. Tobacco Mosaic Virus-Templated Hierarchical Ni/NiO with High Electrochemical Charge Storage Performances. *Electrochim. Acta* **2016**, *220*, 184.

(23) Gerasopoulos, K.; McCarthy, M.; Royston, E.; N Culver, J.; Ghodssi, R. Nanostructured Nickel Electrodes Using the Tobacco Mosaic Virus for Microbattery Applications. *J. Micromech. Microeng.* **2008**, *18* (10), 104003.

(24) Zang, F.; Gerasopoulos, K.; Fan, X. Z.; Brown, A. D.; Culver, J. N.; Ghodssi, R. Real-Time Monitoring of Macromolecular Biosensing Probe Self-Assembly and on-Chip ELISA Using Impedimetric Microsensors. *Biosens. Bioelectron.* **2016**, *81*, 401−407.

(25) Gerasopoulos, K.; Pomerantseva, E.; McCarthy, M.; Brown, A.; Wang, C.; Culver, J.; Ghodssi, R. Hierarchical Three-Dimensional Microbattery Electrodes Combining Bottom-up Self-Assembly and Top-down Micromachining. *ACS Nano* **2012**, *6* (7), 6422−6432.

(26) Mugele, F.; Baret, J.-C. Electrowetting: From Basics to Applications. *J. Phys.: Condens. Matter* **2005**, *17* (28), R705−R774.

(27) Kuiper, S.; Hendriks, B. H. W. Variable-Focus Liquid Lens for Miniature Cameras. *Appl. Phys. Lett.* **2004**, *85* (7), 1128−1130.

(28) Kim, D. Y.; Steckl, A. J. Electrowetting on Paper for Electronic Paper Display. *ACS Appl. Mater. Interfaces* **2010**, *2* (11), 3318−3323.

(29) Samiei, E.; Tabrizian, M.; Hoorfar, M. A Review of Digital Microfluidics as Portable Platforms for Lab-on a-Chip Applications. *Lab Chip* **2016**, *16*, 2376−2396.

(30) Krupenkin, T. N.; Taylor, J. A.; Schneider, T. M.; Yang, S. From Rolling Ball to Complete Wetting: The Dynamic Tuning of Liquids on Nanostructured Surfaces. *Langmuir* **2004**, *20* (10), 3824−3827.

(31) Herbertson, D. L.; Evans, C. R.; Shirtcliffe, N. J.; Mchale, G.; Newton, M. I. Electrowetting on Superhydrophobic SU-8 Patterned Surfaces. *Sens. Actuators, A* **2006**, *130131*, 189−193.

(32) Han, Z.; Tay, B.; Tan, C.; Shakerzadeh, M.; Ostrikov, K. Electrowetting Control of Cassie-to-Wenzel Transitions in Super-hydrophobic Carbon Nanotube-Based Nanocomposites. *ACS Nano* **2009**, *3* (10), 3031−3036.

(33) Royston, E.; Ghosh, A.; Kofinas, P.; Harris, M. T.; Culver, J. N. Self-Assembly of Virus-Structured High Surface Area Nanomaterials and Their Application as Battery Electrodes. *Langmuir* **2008**, *24* (3), 906−912.

(34) Knez, M.; Bittner, A. M.; Boes, F.; Wege, C.; Jeske, H.; Maiβ, E.; Kern, K. Biotemplate Synthesis of 3-Nm Nickel and Cobalt Nanowires. *Nano Lett.* **2003**, *3*, 1079.

(35) Bruckman, M. A.; Liu, J.; Koley, G.; Li, Y.; Benicewicz, B.; Niu, Z.; Wang, Q. Tobacco Mosaic Virus Based Thin Film Sensor for Detection of Volatile Organic Compounds. *J. Mater. Chem.* **2010**, *20* (27), 5715−5719.

(36) Czapar, A. E.; Zheng, Y. R.; Riddell, I. A.; Shukla, S.; Awuah, S. G.; Lippard, S. J.; Steinmetz, N. F. Tobacco Mosaic Virus Delivery of Phenanthriplatin for Cancer Therapy. *ACS Nano* **2016**, *10* (4), 4119−4126.

(37) Koch, C.; Wabbel, K.; Eber, F. J.; Krolla-Sidenstein, P.; Azucena, C.; Gliemann, H.; Eiben, S.; Geiger, F.; Wege, C. Modified TMV Particles as Beneficial Scaffolds to Present Sensor Enzymes. *Front. Plant Sci.* **2015**, *6* (December), 01137.

(38) Xu, W.; Choi, C. H. From Sticky to Slippery Droplets: Dynamics of Contact Line Depinning on Superhydrophobic Surfaces. *Phys. Rev. Lett.* **2012**, *109* (2), 10.1103/PhysRevLett.109.024504.